International Atomic Energy Agency

INDC(EGY)-007
Distr. G+Special

INDC INTERNATIONAL NUCLEAR DATA COMMITTEE

# PERFORMANCE AND MAIN CHARACTERISTIC PARAMETERS OF THE CAIRO FOURIER DIFFRACTOMETER FACILITY AT THE ET-RR-1 REACTOR

R.M.A. Maayouf, I. Abdel-Latif, A. El-Kady,
A. El-Shafey, M. Khalil and Y. El-Shaer

NRC, Atomic Energy Authority
Cairo, Egypt

May 1997

IAEA NUCLEAR DATA SECTION, WAGRAMERSTRASSE 5, A-1400 VIENNA

Printed by the IAEA in Austria
May 1997

INDC(EGY)-007
Distr. G+Special

# PERFORMANCE AND MAIN CHARACTERISTIC PARAMETERS OF THE CAIRO FOURIER DIFFRACTOMETER FACILITY AT THE ET-RR-1 REACTOR*

R.M.A. Maayouf, I. Abdel-Latif, A. El-Kady,
A. El-Shafey, M. Khalil and Y. El-Shaer

NRC, Atomic Energy Authority
Cairo, Egypt

**Abstract**

This report represents the results of measurements performed recently with the Cairo Fourier diffractometer facility (CFDF). The main components of the CFDF were supplied by the IAEA according to the technical assistance project EGY/1/022. The CFDF performance is assessed and the main parameters are given. The neutron guide system attached to the CFDF provides a thermal neutron flux ~$10^6$n/cm$^2$.sec at the sample position; free from fast neutrons and gamma rays background. It has been found, from measurements with different powder samples, that such value of the thermal neutron flux is adequate for neutron diffraction measurements, at scattering angle $2\theta = 90°$ and D values between 0.7Å and 2.5Å; with 52% resolution.

* The main parts of the facility were supplied by the IAEA (Vienna) according to the TC project EGY/1/22.

May 1997

CONTENTS

## 1. INTRODUCTION

One of the most efficient slow neutron scattering techniques, for studying the properties of condensed matter, is that based on the time-of- flight (TOF) method. The TOF measurements require a neutron chopper in order to define a limited time interval during which a neutron spectrum, from the source, is allowed to travel through a certain flight path distance; separates the sample position from the rest of the TOF spectrometer. This allows to study the sample under exceptional condition e.g. at high pressure or temperature where heavy and unmovable sample holders are necessary.

Correlation TOF methods, using either Fourier or pseudorandom beam modulation, have been developed [1,2] for using the available neutron flux in a way more economic, than the usually used Fermi chopper systems, and without deterioration of the resolution. The Fourier approach [3] offers, regardless of resolution requirements, a high duty cycle combined with the possibility of exploiting a large beam area; it allows for a duty ratio up to 50% while the Fermi chopper systems make use only of ~0.1-0.5% of the available neutrons [4]. The Fourier method has been improved by the reverse time-of-flight (RTOF) concept [5,6] which is based on the triggering of the TOF analyzer by the detected neutrons instead of the position of the rotor.

The RTOF technique is particularly useful in Fourier TOF measurements as it provides an inherently on-line way of performing the required spectrum synthesis without any off-line data manipulations. The use of the Fourier RTOF diffractometry, as efficient tool for studying condensed matter at the ET-RR-1 reactor, was assessed in [3]; and the preliminary arrangement to be used at such type of reactor was also given. Further developments of the suggested arrangement were represented in [7-12], along with the main components required for the data acquisition. Moreover, the basic stage of the Cairo Fourier diffractometer facility (CFDF), based on the RTOF concept, was recently installed, as IAEA-TC Project EGY/1/022, at one of the ET-RR-1 reactor horizontal channels.

The present paper presents the facility (CFDF), its performance and main characteristic parameters. Preliminary reports of the facility and first test measurements were given before [13,14].

## 2. THE RTOF DIFFRACTOMETER FACILITY

A schematic diagram of the CFDF at the ET-RR-1 reactor, is represented in Fig.1. Accordingly neutrons emitted, through in-pile collimator, from one of the ET-RR-1 reactor horizontal channels are first guided by the main neutron guide (22m in length); then incident on the Fourier chopper. Neutrons,after the Fourier chopper, pass through

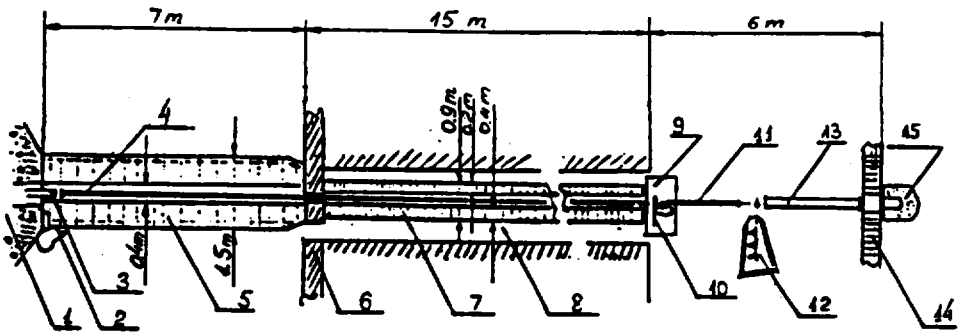


*1 ET-RR-1 Reactor* — *2,5,7, Heavy Concrete Shield*
*3 Inpile Collimator* — *4 Curved Neutron Guide*
*6 Reactor Hall's Wall* — *3 Corridor*
*9 Fourier Chopper Table* — *10 Fourier Chopper*
*11 Straight Neutron Guide* — *12 Detector 13 Evaculated Tabe*
*14 Laboratory Back Wall* — *15 Neutron Beam Catcher*

***Fig.1. A schematic diagram of the CFDF at the ET-RR-1 reactor***

an auxiliary neutron guide (3 m long) to the sample. Neutrons scattered from the sample at 90° are detected by the detector system. The mode of operation, at this stage, is with the detector posit ion at 90° scattering angle. This scattering angle gives the best resolution in space localization of a sample scattering volume and could be used, with high efficiency, for studying the internal stresses in materials; along with neutron diffraction. The arrangement is also equipped with a Fermi chopper which could be used, whenever it is required, for spectrum measurements...etc., The Fermi chopper has been described in details elsewhere [13,14].

### 2.1. The Neutron Guide System

The diffractometer neutron guide system has been especially optimized [3,15] following the same procedure of Ref.[16]; it includes an inpile cone collimator, a main curved neutron guide tube (NGT), 22m long, and an auxiliary straight NGT, 3m long. The in-pile collimator is intended for the preliminary formation of the neutron beam at the input of the main NGT. The collimator is tapered in such a way so that the whole area of the reactor channel's bottom is seen from any point of the main guide input cross-section. The main NGT mirror channel cross-section is about 13.5x90mm$^2$ and its curvature radius is 3385.5m. Besides, the main NGT line-of-sight blocks visibility of the reactor channel's bottom, at its exit with a margin of 3m. This, together, with a considerable length of the NGT leads to a strong suppression of the background of gamma quanta and fast neutrons. The NGT mirror channel walls are made of boron loaded optical glass (2cm thick) coated with a film (2200Å thick) of $^{58}$Ni. The efficiency of boron loaded glass has been confirmed [17], as it reduces the gamma-radiation dose by a factor of 10. The value 1.377Å of the curved NGT characteristic wavelength was chosen considering that the maximum of the distribution of thermal

neutrons, emitted from the ET-RR-1 reactor [18] is at ~1.2Å. In this case the flux at the main guide output [15] and the flux on a sample have the values $\Phi_{out}=1.10^7$ n/cm$^2$s and $\Phi_s=2.10^6$ n/cm$^2$s, respectively. The auxiliary neutron guide, 3 m long, with the same cross-section as the main guide, is placed between the Fourier chopper and the sample table, see Fig. 1. It serves to decrease the flux losses due to the beam divergence on its way to the sample. The optical sections of the auxiliary guide are identical to those of the main one.

The biological shielding around the NGT is constructed mainly from borated polyethelene, lead and a wall of heavy concrete. The thickness of the NGT shield is ~0.55 m for that part (7 m in length) situated in the reactor hall (see Fig.1); the shield of the rest of the NGT (15 m long) is of thickness 0.2 and 0.4 m (see Fig.1). The biological shielding has proved to be efficient in cutting down the gamma ray background to values between 1 m Rh/h and 3 m Rh/h respectively for the reactor hall and corridor (see Fig.1); providing the safety of the working personnel. More details about the NGT facility are given elsewhere [19].

**2.2. The Fourier Chopper**

The Fourier chopper modulates the neutron beam periodically; as illustrated in Fig.2. The chopper consists of a rotating disk having 1024 periods comprising one neutron-absorbing and one neutron-transmitting sector of equal angular width. Close to the rotating disk in the neutron beam is a stator piece having the same pattern as the disk. When the disk is rotating, its slit pattern sweeps over the stator pattern allowing, at its maximum transmission, the absorbing sectors of the rotor to fall in line with the absorbing sectors of the stator thus letting half of the neutron beam intensity pass through the chopper. At its minimum transmission the absorbing sectors of the rotor

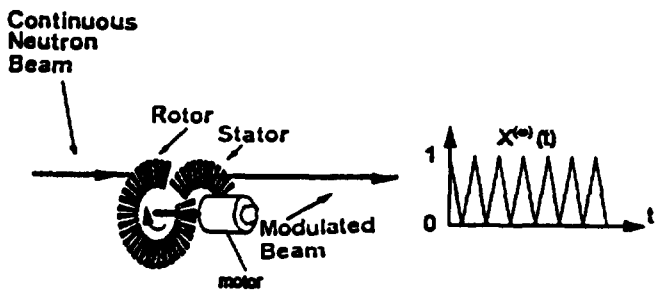


*Fig.2. The Fourier chopper*

fall on the transmiting sectors of the stator thus closing the way of the neutron beam through the chopper. The modulation function of the Fourier chopper should be a saw-tooth wave with the intensity linearly dependent on the rotation angle. The modulation

depth [19] is defined as the ratio of the maximum transmitted intensity (chopper fully open) to the minimum intensity (chopper fully closed). Both the rotor (Φ538 mm disk) and the stator are made of zero-matrix (Ti-Zr-Mn), which in addition to giving an excellent strength to the rotating chopper disk, does not produce any sharp edges to the beam spectrum due to the absence of coherent scattering. The absorbing pattern is made to form a zone of carefully machined sectors. The depth of these sectors is 0.7 mm. These sectors are filled with a mixture containing 60% per weight $Gd_2O_3$ and 40% per weight epoxy resin. The width of the zone is 60 mm and its mean radius is 221mm.

The Fourier chopper has been optimized [12] both for the beam cross-section (13.5x90 $mm^2$) and the minimum loss of intensity due to the gap; between the main NGT and the auxilliary one, necessary for the installation of the chopper in the beam. The chopper mechanical shield has a diaphragm of 17mm x 102 mm made of boron nitride sheet for catching neutrons diverging out of the beam. The scattering of the neutrons from the chopper material has been minimized by machining the stator thickness into 2 mm in the beam area. In addition, the stator and mechanical shield construction have been designed in a way allowing the installation of the chopper into a gap of only 50 mm thus essentially reducing the neutron losses due to beam divergence in the chopper gap.

The rotor is dynamically balanced to a residual unbalance equivalent of 0.61 g at a radius of 150 mm allowing safe rotation of the disk up to 9000 rpm with minimal vibrations. The chopper is rotated by an asynchronous motor controlled with a static inverter. The inverter is connected to a personal computer equipped with a 10 channel Timer/Counter card with a special input for the interrupt. Two connections are applied between the motor control unit and the PC, a serial line (RS 232) for sending commands to the control unit and an interrupt for telling to the PC when the next speed set value is reached. The chopper is run by a program, written specially for such purpose, and can implement any reasonable frequency sweep. Besides, a pick-up signal, tells the momentary position of the chopper, is drawn from an incremental encoder which is attached to the shaft of the chopper motor.

The chopper autocorrelation function measures the quality of the speed control system. The autocorrelation function was first measured, following the procedure of Ref[20], at three maximum speeds of the chopper: 7000, 8000 and 9000 rpm in 20 steps; using a Gaussian window with 1% of Dirichlet. The results are displayed in Fig.3A for first 50 channels (100 μsec.). It is noticeable that the least fluctuations are for 8000 rpm. Accordingly the autocorrelation function was measured at maximum speed of the chopper 8000 rpm using Gaussian window with 1% of Dirichlet; realised by 100 steps. The result of the measurement, is displayed in Fig.3B for the first 100

channels(200μsec) where typical small fluctuations around the main peak are observed. The half width of the autocorrelation function is 7 μsec. Besides the maximum peak-to-peak amplitude of the long-time fluctuations, observed in the measured autocorrelation function (Fig.3B) are on the level of 1% which is acceptable, since in a diffraction pattern measurement it is very seldom to press the statistical fluctuations below this level.

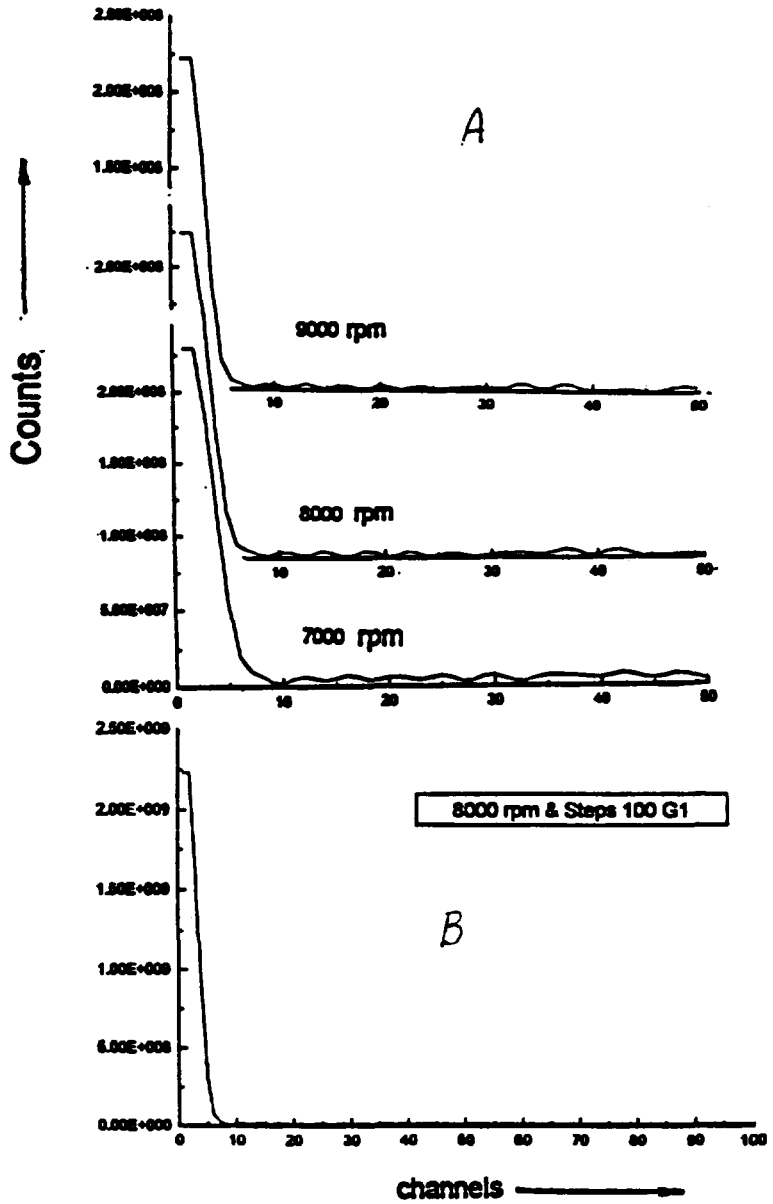


*Fig.3: The chopper autocorrelation function*
*A- at different speeds, B- at 8000 rpm.*

The modulation function and the modulation depth were measured in two ways. First by moving the chopper disk in very small steps (controlled by the micrometer screw attached to its periphery). Thus, the chopper disk position was scanned across one modulation period (with the stator kept fixed) and the transmitted intensity was

measured at equidistant positions of 0.1 mm interval. The results of this measurement are displayed in Fig.4A. The modulation depth resulting from this measurement is 55.3. In the second measurement the chopper disk was kept fixed while the stator was scanned, through another micrometer screw, across one modulation period. The result of this measurement is displayed in Fig.4B. The measurement yielded a modulation depth 47.7. Due to the mechanism of the stator, one modulation period, 1.6 mm, of the chopper corresponds to 8 mm movement of the stator micrometer screw; transmission ratio 1:5. Both measurements (Fig.4 A,B) show a good linearty and confirming a good adjustment of the rotor and the stator. Besides, the weighted average value of the two modulation depth measurements is 55 which can be considered as a very good value when compared to the value 20 for previous similar installations [14] at JINR (Dubna) and PNPI (Gatchina).

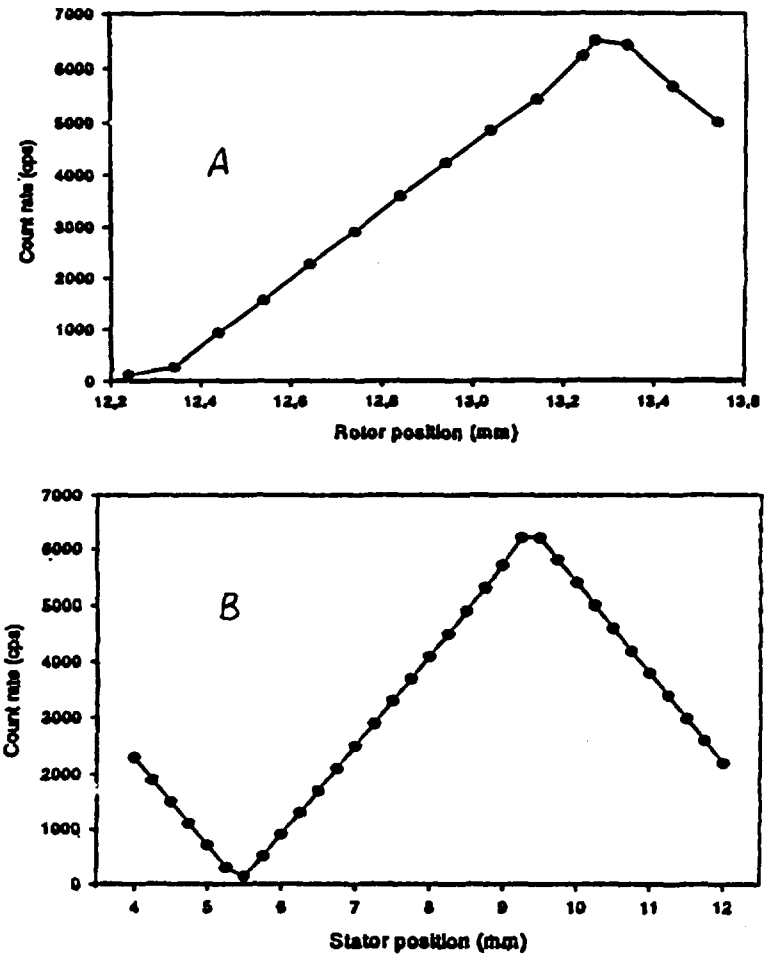


*Fig.4: The modulation function of the chopper*
*A- with fixed stator position, B- with fixed rotor position.*

The final adjustment of the chopper phase was performed by slightly varying the stator position and measuring, at each position, the diffraction pattern of an iron sample (3.9 mm in diameter and 85 mm height). The iron diffraction patterns measured at different stator positions are represented in Fig.5. The final adjustment of the phase was achieved as evident from the diffraction pattern at the bottom of Fig.5, at the stator position 4.9 mm; using the symmetric G1 frequency window.

**2.3. The Detector System**

The $^6$Li-glass (1 mm thick) scintillator (NE-912) is used, in the detector system, for the detection of scattered neutrons as its efficiency for registering thermal neutrons is almost 100%. The detector system is made of pieces small enough to approximate the time focus surface of the scattering neutron trajectories with the desired accuracy so as to attain large solid angle for the scattered neutrons without sacrificing the TOF resolution. The time focusing geometry of the scattered-neutrons detector is described in details in [7]. The detector system is set at 90° scattering angle and optimized for studying the inter nal stresses in materials; along with neutron diffraction measurements. It is an array of four independent (NE-912) scintillation elements, installed at time focusing geometry in order to increase the luminosity. Each detector element contains a light guide, photomultiplier attached to its preamplifier. The sum of the pulses from each individual detector element is used as the detector signal. The detector system applies standard Nuclear Instrument Modules(NIM) for conventional pulse electronics. The surface area of the converter scintillator (NE-912) of each detector element has the dimension 200x200x1 mm$^3$. The detector system aperture is determined by the area of its elements, their angular position and the distance of each of the elements from the sample. The detector system aperture has been precisely calculated [7] by a special program which calculates the detector element positions needed for the fulfillment of the time-focusing conditions. Thus the angular aperture was found equal to $\Omega_D = 5.1 \times 10^{-2}$ steradians.

Three types of light guides are used for transmission of the light flashes from the converter scintillator to the photomultiplier (583006E type). The detector electronics perform preliminary and basic amplification of elctric pulses from the photomultiplier, discriminate the neutron pulses and form them into rectangular shape and adds up the formed pulses from the 4 detector elements. The summed up pulses are then fed to the RTOF analyzer. Fig. 6 represents the pulse-amplitude distribution of each detector element, at the output of the main amplifier, as measured with neutron source (Pu-$\alpha$-Be) whose total flux is $6.7 \times 10^6$n/sec. It is noticeable that good separation, between neutrons and gamma quanta, is achieved for the four detector elements at a discrimination threshold from 1.0-1.5 V .

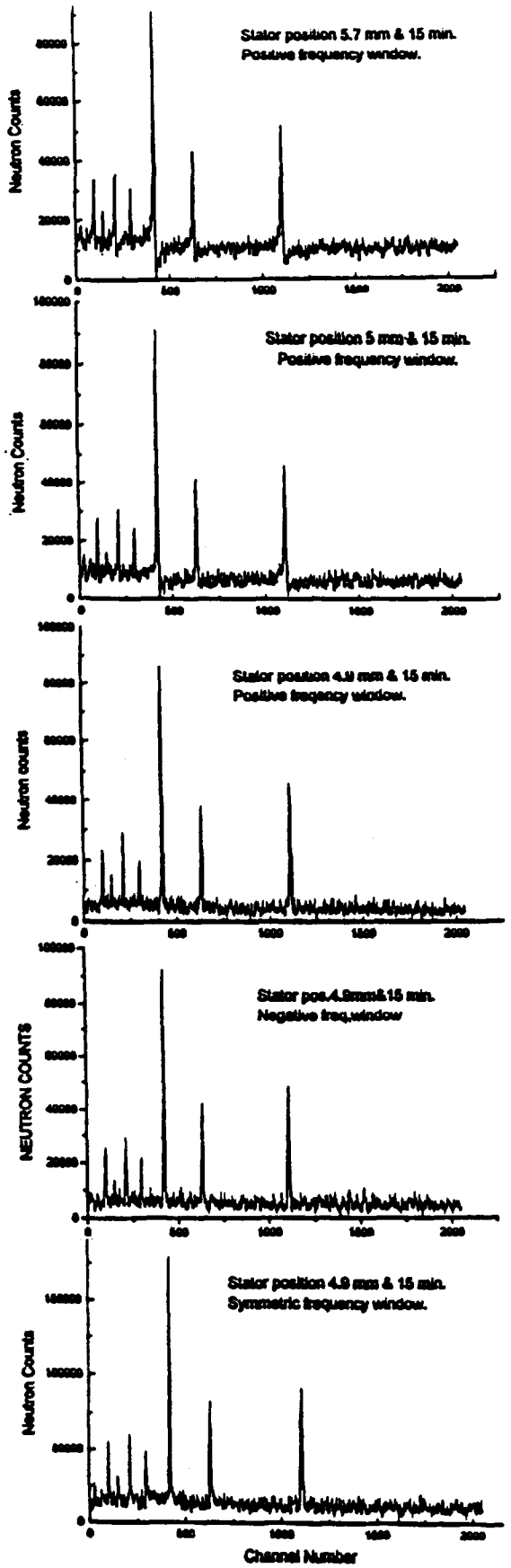


***Fig.5: The iron diffraction patterns measured during the phase adjusment.***

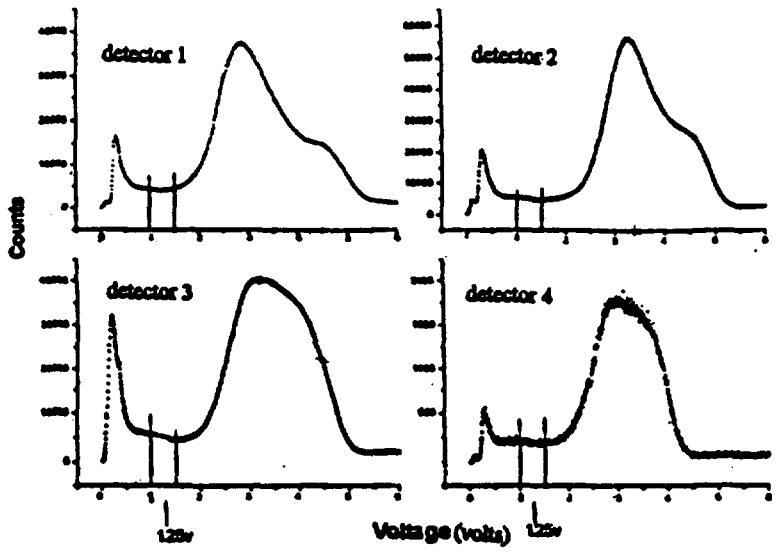


*Fig.6: Pulse amplitude distributions of the detector elements*

## 2.4. The RTOF analyzer arrangement

The electronic system, combined with the Fourier chopper, and used for the RTOF analysis of the measured spectrum is schematically given in Fig.7. Accordingly, the Fourier chopper modulates the neutron beam intensity following $X^{(\omega)}(t)$ law. Simultaneously the chopper optical sensor produces the $Y^{(\omega)}(t)$ reference pick-up signals which are in phase with $X^{(\omega)}(t)$. The rotation speed of the chopper disk determines the modulation frequency ($\omega$) which changes, according to a special frequency window $g(\omega)$, from zero to a maximum value $\Omega$. Besides the RTOF analyzer has a main memory with N channels and a shift register, of the same number of channels, contains a pattern of the reference pick-up signal, which is changing with time over the interval from ($t-\Delta N$) to t. Besides, pulses from a clock generator with a period of $\Delta$(determines the channel width) are connected to the control input of the shift register.

The phase determination accuracy, in the shift register, depends on the stable operation of the clock generator and the value of $\Delta$. Such a distribution of phases, from the shift register, is fed to the analyzer through the moving logic unit at the moment of neutron registeration by the detector. Thus inside the shift register appears a running pattern of rectangular pulses, which exactly reflects the time behaviour of the pick-up signal $Y^{(\omega)}(t-\tau_i)$, where i is equal to the channel number and $\tau_i$ is the time delay ( $\tau_i = i.\Delta$). The functions $X^{(\omega)}(t)$, $Y^{(\omega)}(t)$ and $g(\omega)$ can be selected so that $R(\tau)$ will have a form close to $\delta$ functions (see Fig.7) and its width determins the resolving power of the diffractometer. Consequently, the accumulated data in the RTOF analyser will be given by $Z_i$ which represents the measured spectrum. More details can be found in Refs.[13,16,20].

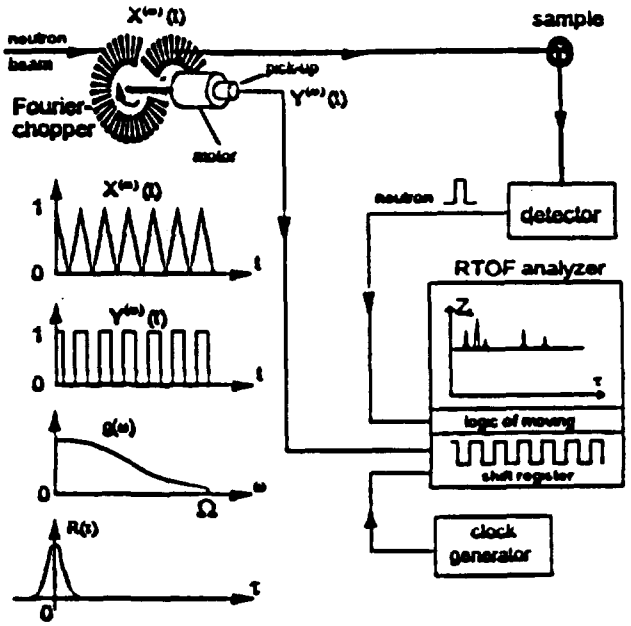


*Fig.7: The electronic system used for the RTOF analysis*

## 3. EXPERIMENTAL MEASUREMENTS

### 3.1. Neutron beam spectrum at the sample position

The classical time-of-flight (TOF)-method with a disk-type Fermi chopper was used for the measurement of the neutron beam spectrum incident on the sample. The disk rotor has 2 radial slits 2.9 mm wide (at $R_0$=200mm) and 80 mm high. The speed of the rotor was 2840 rpm. Such a chopper provides a time-of-flight resolution of 48.8 μs and its transmission is $10^{-3}$. The stator slit of the chopper was vertical in accordance with the position of the sample. One of the detector system elements was used as the detector. It was placed at a distance of (3450±5mm) from the chopper. The measured spectrum of the neutron beam is presented in Fig.(8A). The measurement time was 1 hour, and the channel width of the time-of-flight analyser was 4 μs. The calculated average wavelength of the spectrum is equal to λ= 2.1 Å. An additional measurement of the spectrum with a polycrystalline beryllium sample 120mm thick placed in the way of the beam was performed for calibration of the time-of-flight scale. The result of this measurement is shown in Fig.(8B). Where the well known Be Bragg reflection at 3.952Å is observed.

### 3.2. Integral Neutron Flux Measurements

The present integral neutron flux measurements were performed, using both the calibrated detector and gold activation methods. The calibrated detector measurements were carried out using a $BF_3$ gas filled neutron proportional counter (type LCC

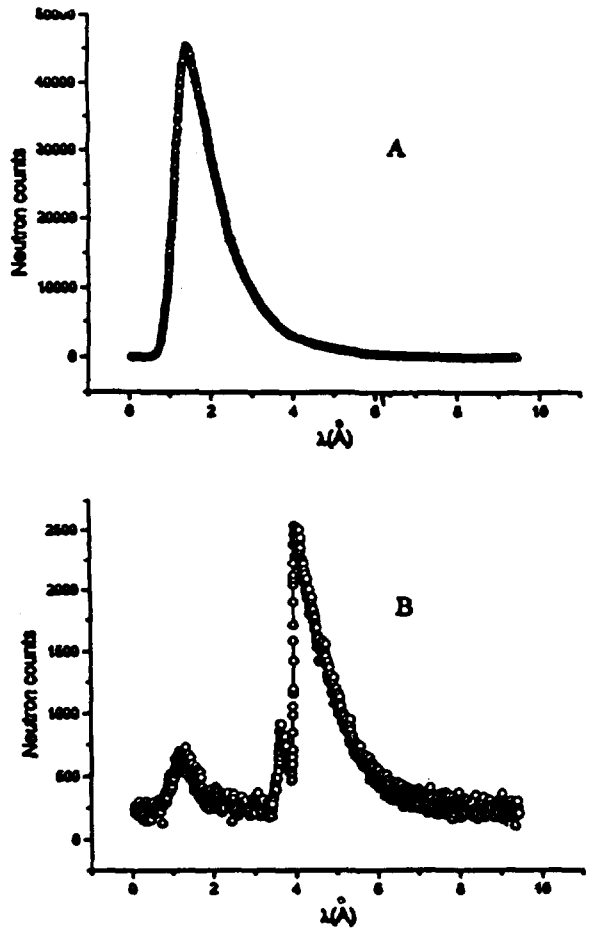


*Fig.8. The measured neutron beam spectra*
*A- direct neutron beam B- Be filtered beam*

Thomson 0.15NH-10) with the efficiency $\varepsilon(1.8) = 0.00495 \pm 0.00030$ at the standard wavelength ($\lambda$=1.8Å); for detector calibration with gold foil. The neutron counter was calibrated [14] for the characteristic wavelength $\lambda^* = 1.35$Å at a chosen mode whose dead time was approximately $\tau = 3$ μsec. Thus, the integral neutron flux was measured at the exit of the curved NGT and at samples' position. The measurement of the neutron flux at the exit of the curved NGT was done, before the Fourier chopper, by placing the counter in the middle of the beam height and using a cadmium slit (3mm in width); allowing open area of the counter $S_D = 3 \times 13.5 mm^2$. The average experimental intensity value, deduced from three values for neutron counts after 10 seconds counting time, and corrected for 3 μsec dead time of the counting system, was $\bar{I}_D$= 15580 n/s. Thus the value of the neutron flux $\Phi_{ex}$ at the exit of the NGT was calculated using the formula:

$$\phi_{ex} = \frac{\overline{I_D}}{S_D \cdot \varepsilon(1.8)} \cdot \frac{\varepsilon(1.8)}{\varepsilon(\lambda)} \qquad (1)$$

where $\bar{\lambda}$ = 2.1 Å is the average wavelength; calculated from the measured neutron spectrum (sec.3.1), and:

$$\frac{\varepsilon(1.8)}{\varepsilon(2.1)} = \frac{1.8}{2.1}, \qquad (2)$$

The calculations, using Eqs(1,2), yielded the value of $\phi_{ex}$=(6.66±0.32)$10^6$n/cm$^2$.s

The measurement of the neutron flux at the sample position was carried out with the vertical counter arrangement using a vertical 3 mm slit. Three measurements were performed; with complete height of the beam (85 mm), at the top half of the beam (42.5±1 mm), and bottom half of the beam (42.5±1 mm). These measurements were performed while the Fourier chopper was rotating. Finally, the value of the neutron flux deduced from the three measurements at the sample position was found to be $\phi_s$ = (1.05±0.05)$10^6$ n/cm$^2$s. The measurement of the neutron flux at the sample position with the non-rotating chopper and in "open" position, yielded the value (2.1±0.01)$10^6$n/cm$^2$s, as expected twice the value of the measurement with the rotating Fourier chopper.

The neutron flux measurements using gold activation methods were performed by activating gold foils (5mm in diameter and ~0.017 gr. in weight) while the Fourier chopper was rotating. The gold foils were fixed at the exits of the curved NGT and the straight NG. The activity of the irradiated gold foils was then measured using an Oxford P-type coaxial hyper pure germanium detector (HPGe) of 56.5 mm crystal diameter and 81.3 mm length; with an active volume ~200 cm$^3$ and a dead layer thickness 600 microns. The flux values were calculated following the procedure of Ref.[21] and using the value of the gold absorption cross-section (98.4 b) given in Ref.[22]. The calculations yielded the values (6.71±0.06)$10^6$n/cm$^2$.s and (1.13±0.04)$10^6$n/cm$^2$.s respectively for the integral neutron flux at the exit of the curved NGT and exit of the straight NGT.

### 3.3. Diffractometer's resolution measurements

The diffraction spectra of standard powder samples were measured in the RTOF mode for studying the diffractometer's resolution. The samples were from α-Fe,

Tungsten carbide (WC) and Diamond; contained in cylinders (5.5mm in diameter and 85mm height) from thin Al foils. These samples were chosen as they satisfy the following conditions:

- The sample's scattering function is close to a delta one; characteristic for perfect structure.
- The scattering intensity, is high enough for good statistics.

Accordingly the diffraction patterns of the samples were measured, at room temperature, with the following setup of the diffractometer:

- Maximum rotation speed of the Fourier chopper: 8000 rpm.
- The frequency window is G3 (Gaussian with oscillation amplitude 3%)
- The RTOF analyzer is set at channel width 2μsec and 1024 μsec delay.

These values are the commonly used ones, with the RTOF measurements, both for strain measurements and crystal structure investigations. The chosen rotation speed allows to decrease the time resolution component of the diffractometer and the use of the G3 frequency window ensures the precise determination of both the peak's position and shape. The measured diffraction patterns are displayed in Fig.(9). Moreover the

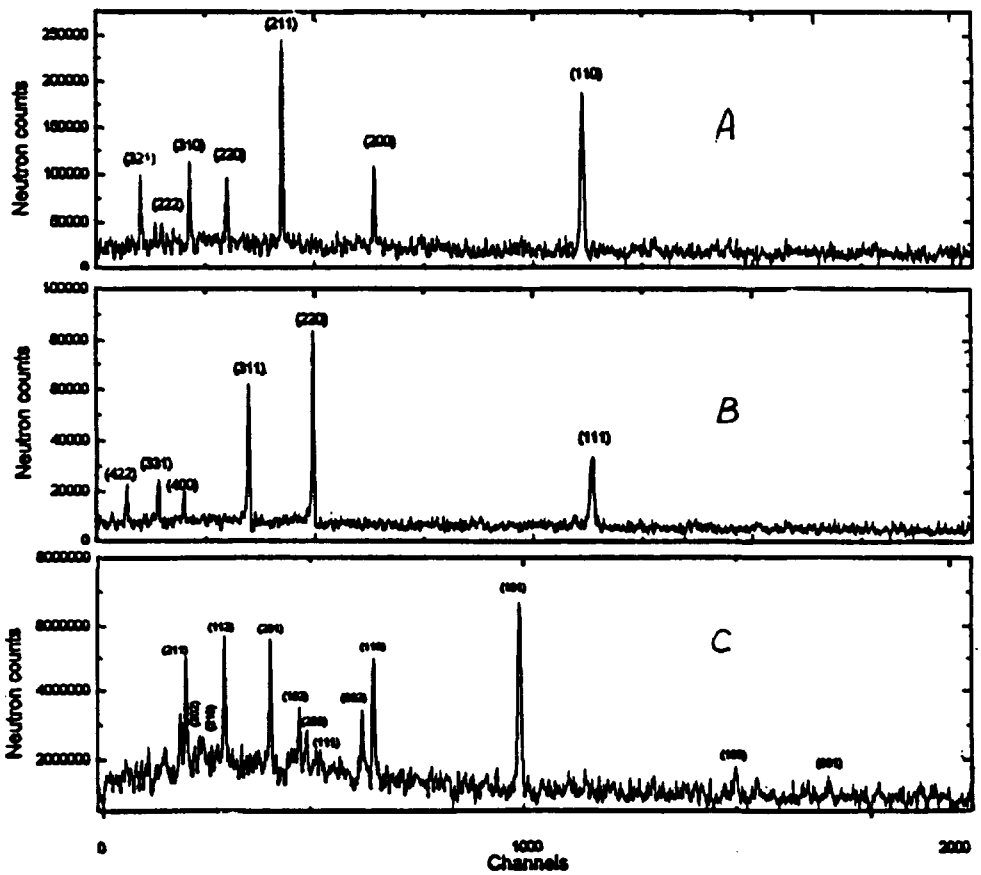


*Fig.9. The measured diffraction patterns*
*A- a-Fe B- diamond C- W.C.*

displayed diffraction patterns were fitted by a Gaussian distribution and the width and position of the observed peaks were defined using the corresponding fit-software. The CFDF software is supplied by a new version of the MRIA code [23] which is based on the Rietveld refinemnt program [24].

## 4. RESULTS AND DISCUSSION

The neutron spectrum measured at the sample position was corrected for:

- The counting losses due to the multichannel analyzer's dead time.
- Absorption and scattering out of the beam in 3.45 m of air between the Fermi chopper and detector.
- The chopper's transmission and resolution.

The corrections were introduced to the measured spectrum following the procedure of Ref.[18]. Moreover, the corrected spectrum yielded the value $2.27 \times 10^6$ n/cm$^2$.s for the integral neutron flux at the sample position.

The values of the measured neutron fluxes are given in table 1. It is noticeable that both flux values measured at the exit of the curved NGT are consistent. Moreover, the flux value obtained from the neutron beam spectrum, at the sample position ($2.27 \times 10^6$ n/cm$^2$.s) is very close to the value $(2.1 \pm 0.01)10^6$ n/cm$^2$.s given in Table 1.

**Table 1: The values of the neutron flux at different neutron beam points**

| point of measurement | fluxes value gold foil activation | flux value calibrated detector |
|---|---|---|
| At the exit of curved NGT | $(6.71 \pm 0.06)10^6$n/cm$^2$.s | $(6.66 \pm 0.32)10^6$ n/cm$^2$.s |
| At the exit of straight NGT | $(1.13 \pm 0.04)10^6$n/cm$^2$.s | |
| At the sample position with rotating Fourier chopper | | $(1.05 \pm 0.05)10^6$n/cm$^2$.s |
| At the sample position with open Fourier chopper | | $(2.1 \pm 0.01)10^6$n/cm$^2$.s |

The dependency between the diffractometer's resolution (FWHM) and $D_{hkl}$(Å), deduced from the peaks in the diffraction patterns displayed in Fig. 9, is presented in

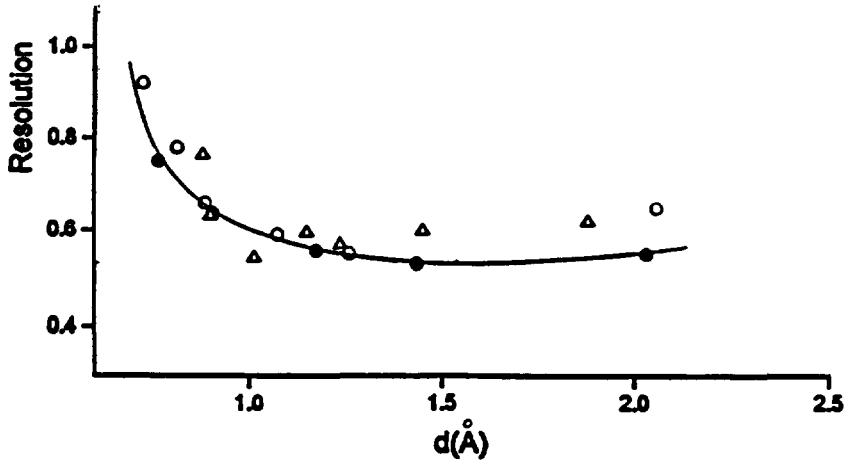


*Fig.10. The diffractometer's resolution*
*o- diamond ●- a-Fe Δ- W.C.*

Fig.10 along with the trend deduced from theoretical calculations of Ref.[13]. It is noticeable that the experimental values, except for the tungsten carbide because of statistics, fit nicely with the theoretical trend yielding a minimum at the value 52% for the resolution of the diffractometer. The latter is slightly lower than the true resolution, since it is a convolution of the instrumental resolution and the natural width of the sample's diffraction line.

The basic parameters of the CFDF are given in table 2, along with those published [25,26] for Mini Sfinks (PNPI-Russia) and FSS (GKSS-Germany) which are similar

**Table 2: Basic parameters of the CFDF compared with similar ones**

| parameter | M.Sfinks PNPI, Gatchina | FSS GKSS, Geesthacht | CFDF Cairo |
|---|---|---|---|
| λ(Å)-range | 1-5 | 1-4 | 1-4 |
| D(Å)-range | 0.5-2.6 | 0.71-2.83 | 0.71-2.83 |
| $\phi_s$(n/cm$^2$.s) | $1.5\times10^7$ | $1.2\times10^6$ | $1.1\times10^6$ |
| $V_s$(cm$^3$) | 5 | 2.125 | 2.125 |
| R(%) | 0.25 | 0.45 | 0.52 |
| Ω(sterad) | 0.09 | 0.0114 | 0.051 |
| $\phi_s V_s \Omega$ | $1.4\times10^5$ | $2.9\times10^4$ | $1.2\times10^5$ |

diffractometers. When comparing the CFDF parameters with those of the Mini Sfinks and FSS facilities one has to bear in mind that they are respectively attached to 18 MW and 5MW reactors while the ET-RR-1 reactor is a 2MW one. Regardless, the luminosity of the CFDF is slightly lower than that of the Mini Sfinks and four times higher than that of the FSS. The resolution of the CFDF is twice less than that of the Mini Sfinks and is very close to the FSS resolution.

## CONCLUSIONS

- The CFDF can be successfully used for high resolution measurements at high count rate of the detector system; significantly saving the measuring time.

- The luminosity of the CFDF makes it possible to obtain neutron diffraction patterns, at scattering angle $2\theta=90^{\circ}$ and D values between 0.7Å-2.5Å; with 52% resolution.

- The further expansion of the CFDF for measurements at $90^{\circ}$ scattering angle, with two detector banks at apposite sides of the incident beam, will allow for the determination of the residual stresses, as well as the phase analysis of polycrystalline materials, which can be widely made use of in steel other metals industry.

## ACKNOWLEDGEMENTS

The authors are grateful to the IAEA (Vienna) for kindly supplying the main components of the CFDF. The assistance of Mrs. K.M.Akhtar and A.Boussaha during different phases of the EGY/1/022 project is deeply acknowledged with thanks. The authors are also grateful to Dr. V.A.Trounov, with his team from PNPI, and Dr. A.Tiitta (VTT) for their valuable assistance during the installation and first test measurements of the CFDF.

**REFERENCES**

[1] GOMPF,F., et al., IAEA Symp. Neutron Inelastic Scattering, Copenhagen 1968, SH-104/77, p. 417-423.
[2] COLWELL,J.F., MILLER,P.M., WHITTEMORE,W.L., IAEA Symp. Neutron Inelastic Scattering, Copenhagen, 1968, SM-104/77, p. 429-437.
[3] MAAYOUF,R.M.A., et al., Report GKSS 91/E/65, Geesthacht, Germany, 1991.
[4] PRIESMEYER,H.G., SCHRODER,J., J. Proc. Mat. Res. Soc. Symp., Materials Research Society, 166 (1990) 299-304.
[5] HIISMAKI,P., et al., Nucl. Inst. & Meth. 126 (1975) 435-443.
[6] POYRY,H., Nucl. Inst. & Meth. 156 (1978) 499-528.
[7] KUDRYASHEV,V.A., TROUNOV,V.A., MAAYOUF,R.M.A., et al., Report LNPI 1732, USSR Academy of Sciences, Leningrad, 1991.
[8] MAAYOUF,R.M.A., TIITTA,A.T., HIISMAKI,P., The RTOF Neutron Diffraction Facility at the ET-RR-1 Reactor, Report VTT Reactor Laboratory, Espoo, Finland, June 1991.
[9] MAAYOUF,R.M.A., et al., Report VTT (Technical Research Centre of Finland), VTT Research Notes-1425, Espoo, 1992.
[10] MAAYOUF,R.M.A., TIITTA,A.T., VTT Research Notes-1502, Espoo, 1993.
[11] MAAYOUF,R.M.A., HIISMAKI,P.E., TIITTA,A.T., The Multipurpose RTOF Fourier Diffractometer at the ET-RR-1 Reactor, Report VTT Reactor Laboratory, Espoo, Nov., 1993.
[12] MAAYOUF,R.M.A., TIITTA,A.T., P.E., HIISMAKI,P.E., VTT Research Notes-1699, VTT, Espoo, 1995.
[13] MAAYOUF,R.M.A., A Fourier RTOF Diffractometer Facility at the ET-RR-1 Reactor, IAEA-SR-198/15, Int. Seminar on Enhancement of Research Reactors Utilization, Bhabha Atomic Research Centre, Bombay, India, 11-15 March, 1996.
[14] TROUNOV,V.A., et al., Report on the Test Experiments of the Multipurpose Diffractometer, Project EGY/1/022, Submitted to the IAEA (Vienna) in April 1996 (Unpublished).
[15] MAAYOUF,R.M.A., El-KADY,A.S., Optimization of a Neutron Guide Facility for the ET-RR-1 Reactor, Sixth Conf. Nucl. Sci. & Appl., 15-20 March, Cairo,1996.
[16] V.A.Trunov et al., LNPI Rep. 1277, USSR Academy of Sciences, Leningrad, 1987.
[17] JACROT,B., Instrumentation for Neutron Inelastic Research, IAEA, Vienna, 1970.
[18] MAAYOUF,R.M.A., et al., Arab. J. Nucl. Sci. & Appl.; 2 (1969) 97.
[19] MAAYOUF,R.M.A., TROUNOV,V.A. KUDRYASHEV,V.A., BULKIN,A., et al., Int. Symp. Neutron Optics and Related Research Facilities NOK'96, 19-21 March, Kumatori, Osaka, Japan, 1996.
[20] TIITTA,A., A Reverse time-of-flight Diffractometer Using a Fourier Chopper, Technical Research Centre of Finland (VTT) Report 27, Espoo, 1980.
[21] LAPP,R.E., ANDREWS,H.L., Nuclear Radiation Physics, 2nd Edition D.H.Menzei, Editor, Prentice-Hall, Inc. New York, 1955.
[22] MUGHABGHAB,S.F., GARBER,D.I., Neutron Cross-sections, BNL 325, 3rd Edition, Brook haven National Laboratory, USA, June 1973.

[23] ZLOKAZOV,V.B., CHERNYSHEV,V.V., J. Appl. Cryst., 25(1992) 447.

[24] RIETVELD,H.M, J.Appl. Cryst, 2(1969) 65 .

[25] TROUNOV,V.A., M.Sfinks Diffractometer at Gatchina Reactor, ICANS-XIII, 13th Meeting of the Int. Collaboration on Advanced Neutron Sources, Oct. 11-14, Paul Scherrer Institute, Switzerland, 1995.

[26] SCHRODER., J. et al., J. of Neutron Research, Vol.2, No.4, 1994 pp.129-141.

Nuclear Data Section
International Atomic Energy Agency
P.O. Box 100
A-1400 Vienna
Austria

e-mail: services@iaeand.iaea.or.at
fax: (43-1)20607
cable: INATOM VIENNA
telex: 1-12645 atom a
telephone: (43-1)2060-21710

online: TELNET or FTP: iaeand.iaea.or.at
username: IAEANDS for interactive Nuclear Data Information System
username: ANONYMOUS for FTP file transfer
For users with Web-browsers: http://www-nds.iaea.or.at